NANO LETTERS

2007
Vol. 7, No. 7
1941−1946

Radiative and Nonradiative Rates of Phosphors Attached to Gold Nanoparticles

T. Soller, M. Ringler, M. Wunderlich, T. A. Klar,* and J. Feldmann

Photonics and Optoelectronics Group, Department of Physics and CeNS, Ludwig-Maximilians-Universität München, Amalienstrasse 54, 80799 Munich, Germany

H.-P. Josel, Y. Markert, A. Nichtl, and K. Kürzinger

Roche Diagnostics GmbH, Nonnenwald 2, 82371 Penzberg, Germany

Received March 15, 2007; Revised Manuscript Received May 6, 2007

ABSTRACT

Gold nanoparticles manipulate the quantum efficiency of phosphorescent molecules, which are attached via biotin–streptavidin recognition at a distance of 4 nm to the nanoparticle surface. Time-resolved luminescence spectroscopy reveals an increase in the radiative as well as in the nonradiative rate of the phosphorescent molecules upon binding to gold nanoparticles. The increase in the radiative rate alone would lead to an increased luminescence quantum yield. However, this effect is outweighed by the distinct enhancement of the nonradiative rate due to energy transfer, resulting in an overall quenching of the luminescence.

The luminescence of chromophores changes when they are placed in close vicinity of gold nanoparticles (AuNPs). This effect allows conjugates of chromophores and AuNPs to be used across a vast spectrum of applications, for example as energy transfer assays for the detection of DNA[1,2] or proteins.[3,4] The net luminescence can either decrease[5] or increase[6,7] depending on how the gold particle affects the chromophore's excitation rate R_{exc}, and the radiative and nonradiative decay rates of its excited state, R_{rad} and R_{nonrad}, which together determine the observed luminescence emission rate R_{emiss}

$$R_{emiss} = R_{exc}\eta \tag{1}$$

Here

$$\eta = \frac{R_{rad}}{R_{rad} + R_{nonrad}} \tag{2}$$

is the quantum efficiency of luminescence which is modified by AuNPs. The relative orientation of a chromophore's molecular dipole moment with respect to the AuNP surface determines whether the radiative rate is increased or decreased.[8] For a tangentially oriented dipole, the radiative rate is diminished because the molecular dipole and the dipole induced on the AuNP radiate out of phase. Additionally, the AuNP increases the nonradiative rate due to energy transfer. Both effects likewise lead to luminescence quenching. In contrast, the radiative rate increases if the dipole is orientated radially toward the AuNP surface. This time the fields of the molecular dipole and the induced dipole interfere constructively. However, the nonradiative rate is increased by energy transfer for radial polarization, as well. A luminescence quenching occurs if the energy transfer is the dominating effect, while the luminescence is enhanced if the increase of R_{rad} prevails. Therefore, a full understanding of the chromophore−AuNP interaction requires the detection of both rates, R_{rad} and R_{nonrad}.

While the effects of AuNPs on neighboring fluorescent molecules have been investigated thoroughly,[5−7] there are only a few corresponding studies that focus on the influence of gold nanoparticles on the luminescent properties of nearby phosphorescent molecules (phosphors) which have a dipole strength that is reduced by orders of magnitude compared to that of fluorophores and consequently phosphors exhibit radiative rates and rates of energy transfer to the gold nanoparticles that are both reduced by orders of magnitude. Phosphors are particularly suitable for biosensing applications, as they allow cutoff of autofluorescence of biological samples by time-gated luminescence detection.[9,10] The phosphorescent metal complexes ruthenium(II) tris(2,2′-bipyridyl) ($Ru(bpy)_3$) and osmium(II) tris(2,2′-bipyridyl) ($Os(bpy)_3$) have been investigated, either adsorbed directly on

10.1021/nl070623b CCC: $37.00
Published on Web 06/13/2007

a gold nanoparticle[11] or bound electrostatically very close to the nanoparticle's surface.[12] Both studies report a luminescence quenching. In the case of the adsorbed phosphors, the quenching was explained by an electron transfer from the phosphors to the AuNP,[11] while for the electrostatically bound phosphors the luminescence decrease was considered to be due to energy transfer.[12] However, details of the luminescence quenching, especially the influence of the AuNP on the radiative and nonradiative rates of the phosphors, have not been discussed. Related studies investigated the luminescence of $Ru(bpy)_3$ close to silver island films on quartz substrates,[13] or close to a two-dimensional layer of noble metal NPs.[14] The catalysis of charge-transfer reactions between phosphors bound very closely to AuNPs has also been investigated.[15]

In this Letter, we examine how AuNPs affect the radiative and nonradiative rates of two phosphors, palladium(II) 5-carboxyphenyl-10,15,20-tris(*p*-sulfophenyl)porphyrin (PdCS3P) and $Ru(bpy)_3$. The phosphors are attached to gold nanoparticles with diameters of 20 or 40 nm via biotin−streptavidin recognition at a distance of approximately 4 nm from the AuNP surface. Time-resolved luminescence spectroscopy reveals an increase of the radiative as well as the nonradiative rate when the phosphors bind to the AuNPs. While the increase of the radiative rate alone would increase the phosphorescence quantum yield, the more prominent increase of the nonradiative rate outweighs this effect, so that in net luminescence quenching occurs.

The energy transfer rate R_{ET} scales with the intrinsic radiative rate $R_{rad,int}$ of the chromophores because both processes depend on the dipole strength. A direct proportionality between $R_{rad,int}$ and the energy transfer rate R_{ET} is found for both radial ($\perp$) and tangential ($\parallel$) dipole orientations[8,16]

$$R_{ET,\perp} = -\frac{R_{rad,int}}{|1-\Delta_\perp|^2}\left(\frac{3c^3\epsilon_m}{2\omega^3 r^3}\right)\times \sum_{n=1}^{\infty}(2n+1)\frac{(n+1)^2}{n}\,\mathrm{Im}\left[\frac{1}{\epsilon+(1+1/n)\epsilon_m}\right]\left(\frac{r}{r+d}\right)^{2n+4} \quad (3)$$

$$R_{ET,\parallel} = -\frac{R_{rad,int}}{|1-\Delta_\parallel|^2}\left(\frac{3c^3\epsilon_m}{4\omega^3 r^3}\right)\times \sum_{n=1}^{\infty}(n+1)(2n+1)\,\mathrm{Im}\left[\frac{1}{\epsilon+(1+1/n)\epsilon_m}\right]\left(\frac{r}{r+d}\right)^{2n+4} \quad (4)$$

Here, $\Delta_\perp$ and $\Delta_\parallel$ denote the so-called image enhancement factors,[16] ω is the angular frequency of the incident light wave, c is the speed of light, ϵ and ϵ_m are the dielectric constants of the gold nanoparticle and the surrounding medium, respectively, r is the particle radius, and d denotes the distance between the phosphor and the AuNP surface. The direct proportionality between $R_{rad,int}$ and R_{ET} was also found by Förster for a purely organic donor−acceptor pair.[17]

Figure 1 shows a scheme of the phosphor−AuNP hybrid system. First, gold nanoparticles with diameters of 20 and 40 nm are functionalized with streptavidin (SA). Remaining gaps in the streptavidin layer are sealed with an excess of bovine serum albumin (BSA) or poly(ethylene glycol) (PEG) in the case of $Ru(bpy)_3$ or PdCS3P, respectively. Therefore, only the outer binding pockets of streptavidin are available for biotin recognition. The phosphors $Ru(bpy)_3$ and PdCS3P are modified with the spacer molecule 1,8-diamino-3,6-dioxaoctane (DADOO) and subsequently functionalized with biotin (Bi). The biotinylated compounds are denoted by Ru(bpy)$_3$-Bi and PdCS3P-Bi. The Ru(bpy)$_3$-Bi and the nonbiotinylated $Ru(bpy)_3$ show the same absorption as well as emission intensities. Only a minor red shift of 7 nm is observed for the spectral positions of the absorption and emission upon biotinylation. Thus, the biotinylation does not significantly affect the optical properties of the phosphors. The mean adhesion time of the biotinylated phosphors in the binding pockets is appreciably longer than the luminescence lifetimes because of the strength of the biotin−streptavidin bond. Therefore, the connection between the phosphors and the AuNPs is considered static on the experimental time scale. However, the orientation of the phosphor with respect to the AuNP surface may change during the lifetime of a molecular excitation because of some

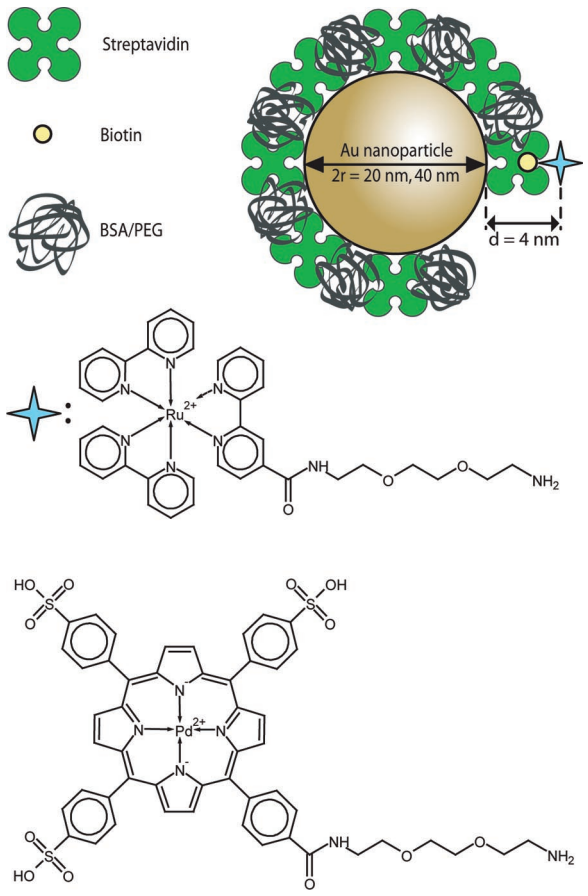

Figure 1. Gold nanoparticles with diameters ($2r$) of 20 and 40 nm are functionalized with streptavidin (SA). Remaining gaps are sealed with either BSA or PEG. The biotinylated phosphorescent metal complexes $Ru(bpy)_3$ and PdCS3P are attached to the nanoparticles via streptavidin−biotin recognition. The phosphors are situated approximately 4 nm from the particles' surface.

orientational flexibility of the biotin−streptavidin bond and the DADOO linker.

For sample preparation, the concentrations of phosphors and gold nanoparticles are determined from extinction measurements, assuming literature values of the extinction coefficient for $Ru(bpy)_3$[18] and Pd−tetra(*p*-sulfophenyl)-porphin[19] which is structurally very similar to PdCS3P. Extinction cross sections of the AuNPs were calculated using Mie theory.[20] In a typical sample preparation process, 100 μL of a 1.7 μM $Ru(bpy)_3$-Bi solution in 20 mM Tris−HCl buffer is added to 2000 μL of 0.84 nM BSA-free solution of 20 nm AuNPs in a quartz cuvette. The mixture is subsequently diluted by adding 900 μL of pure Tris−HCl buffer solution. Excess BSA is removed from the buffer solution by dialysis to avoid that the hydrophobic biotinylated phosphors interact nonspecifically with unbound BSA. Samples containing PdCS3P-Bi are degassed with argon for 30 min before and during the measurements because PdCS3P-Bi is very sensitive to oxygen quenching. All investigations have been carried out in aqueous solution (pH 7.5) at room temperature to match biological conditions. The solutions are incubated for 45 min to ensure that the samples are in equilibrium condition.

Time-integrated photoluminescence spectra are measured with a Varian Cary Eclipse fluorescence spectrophotometer, and extinction spectra are recorded by a Varian Cary50 UV−vis spectrophotometer. Time-resolved measurements are carried out with a PicoQuant FluoTime 200 fluorescence lifetime spectrometer; the signals are detected with a photomultiplier tube. Samples containing $Ru(bpy)_3$-Bi are excited at 470 nm with a PicoQuant LDH-P-C-470B pulsed diode laser (pulse length ca. 500 ps, repetition rate 200 kHz), and the luminescence decay is recorded in time correlated single photon counting (TCSPC) mode. The PdCS3P-Bi samples are excited at 405 nm with pulses from a xenon flash lamp (pulse length ca. 400 ns, repetition rate 300 Hz), and detection of the decay profile is accomplished by multichannel scaling.

Prior to the discussion of the hybrid systems, we show that the binding between the biotinylated phosphors and streptavidin itself does not significantly affect the optical properties of the phosphors. In recent publications, a pronounced luminescence enhancement (factor 1.2−1.6) upon binding to avidin is reported for phosphorescent ruthenium(II) complexes with either a directly or a closely attached biotin moiety.[21−23] However, in the present case the spacer DADOO separates the biotin subunit and the chromophoric part and control experiments without AuNPs show only a small luminescence enhancement of 8% when $Ru(bpy)_3$-Bi is bound to streptavidin. For PdCS3P-Bi no change of the luminescence strength was observed after addition of streptavidin. Therefore, the influence of SA on the phosphors is negligible in the present case.

Three different phosphor−AuNP hybrid systems are discussed in this Letter: $Ru(bpy)_3$-Bi on $2r = 20$ nm AuNPs, $Ru(bpy)_3$-Bi on $2r = 40$ nm AuNPs, and PdCS3P-Bi on $2r = 20$ nm AuNPs. A concentration series is performed in order to ensure the functionality of the bond between the

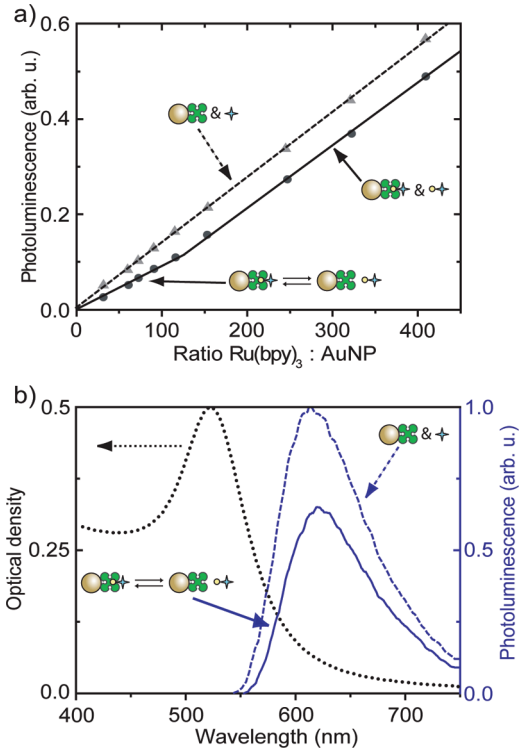

Figure 2. (a) Concentration series of $Ru(bpy)_3$ with 20 nm AuNPs. The number of $Ru(bpy)_3$ molecules per nanoparticle is increased stepwise at a fixed concentration of AuNPs. The luminescence of nonfunctionalized $Ru(bpy)_3$ (triangles) depends linearly on the dye concentration, while a change of the slope is observed in the series of the biotinylated derivative (circles) at 120 dyes per AuNP, representing the maximum number of phosphors which can bind to one particle. (b) Time-integrated extinction spectrum of the nanoparticle solution (dotted line) as well as photoluminescence spectra of biotinylated (solid line) and non-biotinylated (dashed line) $Ru(bpy)_3$, both in presence of AuNPs. The phosphor concentrations correspond to ca. 100 phosphors per AuNP.

phosphors and the nanoparticles. For that purpose, the amount of phosphor molecules is raised stepwise while the number of AuNPs is kept constant. The circles in Figure 2a show this series of measurements for the hybrid system composed of $Ru(bpy)_3$-Bi and 20 nm AuNP. As long as there are fewer phosphors offered than binding sites available, the phosphors are able to attach to the AuNPs and their luminescence is quenched. Therefore, the increase of the luminescence with $Ru(bpy)_3$-Bi concentration is less steep in the case of the hybrid system (Figure 2a, circles), compared to the case of non-biotinylated $Ru(bpy)_3$ (Figure 2a, triangles). All binding sites are saturated at the critical concentration of 120 $Ru(bpy)_3$-Bi per AuNP, and $Ru(bpy)_3$-Bi added in excess is not quenched by the AuNPs. Therefore, the slope in the phosphorescence intensity curve changes at 120 $Ru(bpy)_3$-Bi per AuNP. The experimentally determined saturation concentration is in very good agreement with the calculated number of 75 SA molecules on each AuNP (based on the available surface area per AuNP) and the assumption that there are in average 1.5 accessible biotin binding sites on each SA. Note that the strict linear dependence of the fluorescence in the range from 0 to 120 phosphors per AuNP indicates that no concentration quenching takes place.

Figure 2b shows the optical density spectrum of the gold nanoparticle solution (dotted line). The plasmon peak of the AuNPs can be clearly seen at a wavelength of 523 nm.[24] Further, the figure shows time-integrated luminescence spectra of the ($Ru(bpy)_3$-Bi)/(20 nm AuNP) hybrid system (solid blue line) and of a reference solution (dashed line), containing non-biotinylized $Ru(bpy)_3$ and AuNPs of the same concentrations as in the hybrid system. The $Ru(bpy)_3$ concentrations in both samples are chosen to correspond to 100 phosphors per nanoparticle. We observe that the phosphorescence of the hybrid system is quenched by about 38% in comparison to the reference. The geometry of the streptavidin molecules and the biotinylated complexes defines an average distance of 4 nm between the chromophoric parts of the dyes and the gold surface (Figure 1). This distance is far too large for an electron transfer from the $Ru(bpy)_3$ to the AuNP, so electron transfer cannot cause the luminescence quenching. Further, streptavidin changes the optical properties of the phosphors only marginally as explained above. Therefore we conclude that energy transfer and the manipulation of the phosphors' radiative decay rates by the gold nanoparticles must account for the changed luminescence yield. As will be discussed later, the actual quenching efficiency is much larger than 38% as observed in the time-integrated studies, because the majority of the remaining luminescence intensity is caused by unbound phosphors which are in a dynamic equilibrium with the bound species.

Before we turn to the time-resolved optical emission transients of the phosphor−AuNP hybrid system, we will discuss the time-resolved transients of the isolated components first. A pure solution of gold nanoparticles shows a pulsed emission at $t = 0$ (dotted line in Figure 3a). From a spectral analysis we conclude that this fast emission signal is predominantly due to a Raman emission background from the buffer solution. Time-resolved luminescence measurements on the pure phosphor solutions reveal monoexponential decays with lifetimes of 380 ns for $Ru(bpy)_3$-Bi and 450 μs for PdCS3P-Bi. Considering the experimentally determined quantum efficiencies η of 0.027 for $Ru(bpy)_3$-Bi and 0.028 in the case of PdCS3P-Bi, we obtain the intrinsic radiative rates $R_{rad} = 7.1 \times 10^4\ s^{-1}$ for $Ru(bpy)_3$-Bi and $R_{rad} = 62\ s^{-1}$ for PdCS3P-Bi. Accordingly, the intrinsic nonradiative decay rates amount to $R_{nonrad} = 2.6 \times 10^6\ s^{-1}$ for $Ru(bpy)_3$-Bi and $R_{nonrad} = 2.2 \times 10^3\ s^{-1}$ for PdCS3P-Bi.

Figure 3a shows the emission transient of the ($Ru(bpy)_3$-Bi)/(20 nm AuNP) hybrid. We can identify three components in the decay profile.[5] First, a very fast emission signal at $t = 0$ is observed which shows a peak intensity identical to the pure gold nanoparticle solution (dotted line) due to Raman scattering from the buffer. Second, we observe a long-lived component with a decay time similar to that of free $Ru(bpy)_3$ dyes. This is illustrated by the dashed line in Figure 3a, which represents a single-exponential decay with a time constant $\tau = 380$ ns. Therefore, this component can be attributed to unbound $Ru(bpy)_3$-Bi molecules. Although the streptavidin−biotin bond is very strong, functionalization of biotin with a large metal complex weakens the affinity,[25] which leads to a nonvanishing fraction of free dyes in thermal

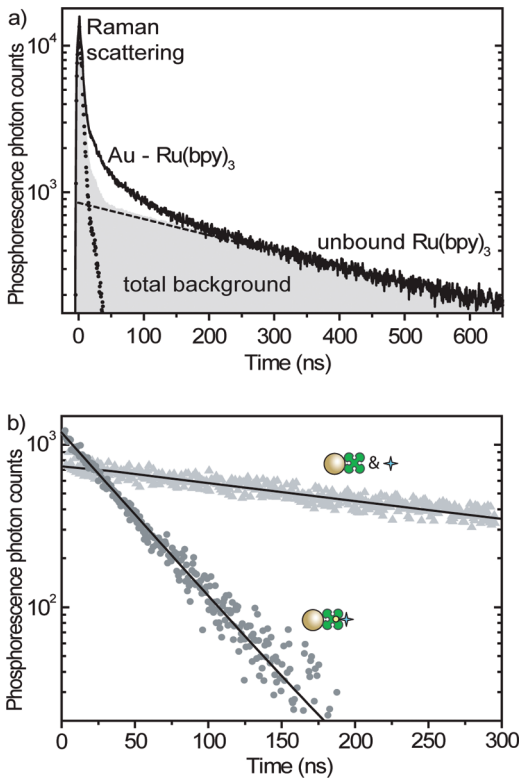

Figure 3. Time-resolved luminescence transients of $Ru(bpy)_3$ bound to 20 nm AuNP. (a) The raw data (black line) are the sum of the signal from phosphors bound to gold nanoparticles and background. The background (gray area) is made up of Raman scattering from the buffer (dotted line) and unmodified phosphorescence from unbound dyes (dashed line). (b) Comparison of the transients of the free $Ru(bpy)_3$ in the reference solution (triangles) and the $Ru(bpy)_3$-Bi−AuNP composite (circles) after removal of background signals. Lines are single-exponential fits.

equilibrium with the bound species. Further, a small percentage of non-biotinylated $Ru(bpy)_3$ may have persisted throughout the synthesis and purification of $Ru(bpy)_3$-Bi. Subtraction of these short- and long-lived background components from the raw transient of the hybrid system yields the luminescence decay profile of the bound phosphors. Further, we take into account a change in the absorption cross section due to the presence of the gold nanoparticles. This is achieved by calculating R_{rad} at the excitation wavelength using the Gersten−Nitzan theory and assuming that absorption and emission probabilities are proportional.[5] The resulting correction factors are less than 2 for all three composite systems under consideration.

The decay signal resulting after these corrections is shown in Figure 3b for $Ru(bpy)_3$-Bi attached to AuNPs with 20 nm in diameter (circles). The luminescence turns out to decay monoexponentially for all phosphor−AuNP systems under consideration. Compared to the phosphorescence lifetimes of unbound $Ru(bpy)_3$ (triangles), a substantial lifetime shortening is observed. We obtain a lifetime $\tau = 44$ ns for $Ru(bpy)_3$-Bi on 20 nm AuNP, and in analogous experiments we obtain $\tau = 42$ ns for $Ru(bpy)_3$-Bi on 40 nm AuNP and $\tau = 82$ μs for PdCS3P-Bi on 20 nm AuNP. From the experimentally obtained lifetimes, we deduce the overall decay rate $R = \tau^{-1}$ of the bound phosphors. The overall

Table 1. Comparison of the Experimental Data for the Nonradiative and Radiative Rates with the Predictions of the Gersten−Nitzan Model for Tangential, Radial and Random Orientation of the Dye's Dipole Moment toward the Gold Surface

		Gersten−Nitzan theory		
system	experiment $R_{\mathrm{nonrad}}^{\mathrm{exp}}$ (s^{-1})	$R_{\mathrm{nonrad,random}}^{\mathrm{GN}}$ (s^{-1})	$R_{\mathrm{nonrad,\parallel}}^{\mathrm{GN}}$ (s^{-1})	$R_{\mathrm{nonrad,\perp}}^{\mathrm{GN}}$ (s^{-1})
$Ru(bpy)_3$	$(2.6 \pm 0.1) \times 10^6$	2.6×10^6	2.6×10^6	2.6×10^6
$Ru(bpy)_3$-20 nm AuNP	$(2.3 \pm 0.1) \times 10^7$	2.4×10^7	1.6×10^7	4.1×10^7
$Ru(bpy)_3$-40 nm AuNP	$(2.4 \pm 0.1) \times 10^7$	2.4×10^7	1.7×10^7	3.8×10^7
PdCS3P	$(2.2 \pm 0.1) \times 10^3$	2.2×10^3	2.2×10^3	2.2×10^3
PdCS3P-20 nm AuNP	$(1.2 \pm 0.1) \times 10^4$	1.0×10^4	0.71×10^4	1.6×10^4

		Gersten−Nitzan theory		
system	experiment $R_{\mathrm{rad}}^{\mathrm{exp}}$ (s^{-1})	$R_{\mathrm{rad,random}}^{\mathrm{GN}}$ (s^{-1})	$R_{\mathrm{rad,\parallel}}^{\mathrm{GN}}$ (s^{-1})	$R_{\mathrm{rad,\perp}}^{\mathrm{GN}}$ (s^{-1})
$Ru(bpy)_3$	$(7.1 \pm 0.2) \times 10^4$	7.1×10^4	7.1×10^4	7.1×10^4
$Ru(bpy)_3$-20 nm AuNP	$(11 \pm 1) \times 10^4$	15×10^4	0.51×10^4	44×10^4
$Ru(bpy)_3$-40 nm AuNP	$(13 \pm 2) \times 10^4$	27×10^4	0.33×10^4	81×10^4
PdCS3P	$(6.2 \pm 0.2) \times 10^1$	6.2×10^1	6.2×10^1	6.2×10^1
PdCS3P-20 nm AuNP	$(6.8 \pm 1.0) \times 10^1$	10×10^1	1.2×10^1	29×10^1

decay rate is the sum of the radiative and the nonradiative rate: $R = R_{\mathrm{rad}} + R_{\mathrm{nonrad}}$. Since the radiative rate is directly proportional to the luminescence signal $I(0)$ at time $t = 0$, R_{rad} of the hybrid systems can be deduced from the time-resolved spectra by comparing $I(0)$ of bound and unbound phosphors and multiplying this ratio with the phosphor's known intrinsic radiative rate.[5,26] The nonradiative rate R_{nonrad} is subsequently calculated by subtracting R_{rad} from the overall decay rate R. Table 1 shows the obtained radiative and nonradiative rates for all composite systems under consideration. We find a slight increase of R_{rad} and a 10-fold increase of R_{nonrad} for all hybrid systems. The increase of the nonradiative rate is due to an energy transfer to the AuNP. On the one hand, the increase of the radiative rate would increase the phosphorescence quantum yield, but on the other hand the more prominent increase of the nonradiative rate outweighs this effect, so that a net luminescence quenching occurs.

The radiative and nonradiative rates calculated with the Gersten−Nitzan theory are also listed in Table 1 for radial ($\perp$), tangential ($\parallel$), and random dipole orientations. The rates for random polarization are obtained by averaging the rates for the radial and the tangential case, taking into account the 2-fold degeneracy of the tangential orientation. On comparison of the experimental results with the Gersten−Nitzan model, a uniformly tangential ($\parallel$) orientation of the phosphors' dipole moments can be ruled out, because theory predicts a reduction of R_{rad} in the presence of AuNPs, while we measure an increase of R_{rad} (Table 1). However, the measured increase of R_{rad} is too small to be explained by a purely radial dipole orientation, as shown by a comparison of $R_{\mathrm{rad}}^{\mathrm{exp}}$ with the theoretical values $R_{\mathrm{rad,\perp}}^{\mathrm{GN}}$. Best agreement with the Gersten−Nitzan theory is achieved by the assumption of a randomly distributed orientation of the phosphors, which is indeed plausible, as the streptavidin−biotin linkage and especially the DADOO spacer undergo rotational motion on a time scale much faster than the lifetime of the phosphor. It can further be seen that the rate of energy transfer scales with R_{rad}, according to eq 3 and eq 4. The intrinsic radiative rate $R_{\mathrm{rad,int}}$ of $Ru(bpy)_3$ is 3 orders of magnitude larger compared to $R_{\mathrm{rad,int}}$ of PdCS3P and, consequently, the energy transfer rate R_{ET} of the $Ru(bpy)_3$−20 nm AuNP hybrid system (calculated as the difference of R_{nonrad} with and without AuNP) is 3 orders of magnitude larger than R_{ET} of the PdCS3P−20 nm AuNP composite, as well.

Table 2. Quantum Yields and Quenching Efficiencies of the Pure Dyes and the Dye−AuNP Hybrid Systems.

system	quantum yield	% quenching efficiency
$Ru(bpy)_3$	2.7×10^{-2}	
$Ru(bpy)_3$−20 nm AuNP	5.0×10^{-3}	81
$Ru(bpy)_3$−40 nm AuNP	5.4×10^{-3}	80
PdCS3P	2.8×10^{-2}	
PdCS3P−20 nm AuNP	5.6×10^{-3}	80

Table 2 lists the quenching efficiencies as well as the quantum yields (eq 2) of the bound species based on the experimentally determined rates. The quenching efficiency is approximately 80% for all three dye−AuNP composites. Interestingly, the luminescence of $Ru(bpy)_3$ is quenched slightly stronger by 20 nm AuNPs than by 40 nm AuNPs. This result is surprising at first, as one would intuitively expect a more efficient energy transfer in the case of the 40 nm colloids due to their larger absorption cross section. However, the increase in R_{nonrad} is almost identical for both systems, while the enhancement of the radiative rate, which counteracts the quenching of luminescence, is more pronounced for the 40 nm particles (see Table 1).

In conclusion, we have shown that the luminescence of the phosphors $Ru(bpy)_3$ and PdCSP3 is considerably quenched in the vicinity of gold nanoparticles due to energy transfer, which adds to the nonradiative rate. Further, we observe a slight increase in the radiative rate which counteracts luminescence quenching. However, as the energy transfer is always the more prominent effect in the investigated hybrid systems, a net quenching of the luminescence occurs. Both

rates R_{rad} and R_{nonrad} can be explained best within the framework of the Gersten−Nitzan theory if a random orientation of the dipole moments of the phosphors is assumed. Our findings are relevant for molecular recognition sensors based on the quenching of long-lived phosphorescence. Quenching of triplet states in phosphors is also relevant in optoelectronics and specifically in spintronics.

Acknowledgment. We thank Dr. J. Koci for the synthesis of the biotin functionalized phosphors and A. Helfrich and W. Stadler for excellent technical assistance. Financial support by the Bayerische Forschungsstiftung is gratefully acknowledged.

Note Added After ASAP Publication. This Letter was published ASAP on June 13, 2007. A correction has been made to reference 15. The correct version was published on July 3, 2007.

References

(1) Dubertret, B.; Calame, M.; Libchaber, A. J. *Nat. Biotechnol.* **2001**, *19*, 365.
(2) Maxwell, D. J.; Taylor, J. R.; Nie, S. *J. Am. Chem. Soc.* **2002**, *124*, 9606.
(3) Aslan, K.; Pérez-Luna, V. H. *J. Fluoresc.* **2004**, *14*, 401.
(4) Ao, L.; Gao, F.; Pan, B.; He, R.; Cui, D. *Anal. Chem.* **2006**, *78*, 1104.
(5) Dulkeith, E.; Morteani, A. C.; Niedereichholz, T.; Klar, T. A.; Feldmann, J.; Levi, S. A.; van Veggel, F. C. J. M.; Reinhoudt, D. N.; Möller, M.; Gittins, D. I. *Phys. Rev. Lett.* **2002**, *89*, 203002.
(6) Anger, P.; Bharadwaj, P.; Novotny, L. *Phys. Rev. Lett.* **2006**, *96*, 113002.
(7) Kühn, S.; Hakanson, U.; Rogobete, L.; Sandoghdar, V. *Phys. Rev. Lett.* **2006**, *97*, 017402.
(8) Gersten, J.; Nitzan, A. *J. Chem. Phys.* **1981**, *75*, 1139.
(9) Beverloo, H. B.; van Schadewijk, A.; van Gelderen-Boele, S.; Tanke, H. J. *Cytometry* **1990**, *11*, 784.
(10) de Haas, R. R.; van Gijlswijk, R. P. M.; van der Tol, E. B.; Veuskens, J.; van Gijssel, H. E.; Tijdens, R. B.; Bonnet, J.; Verwoerd, N. P.; Tanke, H. J. *J. Histochem. Cytochem.* **1999**, *47*, 183.
(11) Glomm, W. R.; Moses, S. J.; Brennaman, M. K.; Papanikolas, J. M.; Franzen, S. *J. Phys. Chem. B* **2005**, *109*, 804.
(12) Huang, T.; Murray, R. W. *Langmuir* **2002**, *18*, 7077.
(13) Gryczynski, I.; Malicka, J.; Holder, E.; DiCesare, N.; Lakowicz, J. R. *Chem. Phys. Lett.* **2003**, *372*, 409.
(14) Tanaka, H.; Mitsuishi, M.; Miyashita, T. *Chem. Lett.* **2005**, *34*, 1246.
(15) Pramod, P.; Sudeep, P. K.; Thomas, K. G.; Kamat, P. V. *J. Phys. Chem. B* **2006**, *110*, 20737.
(16) Dulkeith, E. Optische Charakterisiserung von Hybridsystemen aus Gold Nanopartikeln und Farbstoffmolekülen. Ph.D. Thesis, Ludwig-Maximilians-Univesität, München, 2004.
(17) Förster, T. *Z. Naturforsch.* **1949**, *4a*, 321.
(18) Roundhill, D. M. *Photochemistry and Photophysics of Metal Complexes*; Plenum Press: New York, 1994.
(19) Sapunov, V. V.; Egorova, G. D. *J. Appl. Spectrosc.* **1991**, *54*, 427.
(20) Mie, G. *Ann. Phys.* **1908**, *3*, 25.
(21) Lo, K. K. W.; Hui, W. K.; Ng, D. C. M. *J. Am. Chem. Soc.* **2002**, *124*, 9344.
(22) Slim, M.; Sleiman, H. F. *Bioconjugate Chem.* **2004**, *15*, 949.
(23) Delahaye, S.; Loosli, C.; Liu, S. X.; Decurtins, S.; Labat, G.; Neels, A.; Loosli, A.; Ward, T. R.; Hauser, A. *Adv. Funct. Mater.* **2006**, *16*, 286.
(24) Kreibig, U.; Vollmer, M. *Optical Properties of Metal Clusters*; Gonser, U., Osgood, R. M., Panish, M. B., Sakaki, H., Eds.; Springer-Verlag: Berlin, 1995.
(25) Loosli, A. Investigation of Second Coordination Sphere Interactions Between Biotinylated Coordination Complexes and (Strept)Avidin: CD Spectroscopy as a Powerful Tool for Stability Constant Determinations. Ph.D. Thesis, University of Neuchatel, Neuchatel, 2004.
(26) Aussenegg, F. R.; Leitner, A.; Lippitsch, M. E.; Reinisch, H.; Riegler, M. *Surf. Sci.* **1987**, *189*, 935.

NL070623B